DOI: 10.1002/ ((please add manuscript number))

Article type: Full Paper

Bistetracene Thin Film Polymorphic Control to Unravel the Effect of Molecular Packing on Charge Transport

*Edmund K. Burnett, Jack Ly, Muhammad R. Niazi, Lei Zhang, Samantha R. McCuskey, Aram Amassian, Detlef-M. Smilgies, Stefan C. B. Mannsfeld, and Alejandro L. Briseno**

Edmund K. Burnett, Jack Ly, Dr. Lei Zhang, Samantha R. McCuskey, Prof. Alejandro L. Briseno

Department of Polymer Science and Engineering

University of Massachusetts Amherst

Amherst, MA, 01003, USA

E-mail: abriseno@mail.pse.umass.edu

Muhammad R. Niazi, Prof. Aram Amassian

Physical Science and Engineering Division

King Abdullah University of Science and Technology (KAUST)

Thuwal, 23955-6900, Saudi Arabia

Dr. Detlef-M. Smilgies

Cornell High Energy Synchrotron Source

Cornell University

Ithaca, NY, 14853, USA

Stefan C. B. Mannsfeld

Center for Advanced Electronics Dresden

Dresden University of Technology

Dresden, 01062, Germany

Keywords: organic semiconductors, polymorphism, bistetracene, solvent vapor annealing

Abstract

Polymorphism, the ability for a given material to adopt multiple crystalline packing states, is a powerful approach for investigating how changes in molecular packing influence charge transport within organic semiconductors. In this study, we isolate and characterize a new "thin film" polymorph of the high-performance, p-type small molecule N-octyldiisopropylsilyl acetylene bistetracene (BT). Structural changes in the BT films were monitored using static and *in-situ* grazing-incidence X-ray diffraction (GIXD). The diffraction data, combined with simulation and crystallographic refinement calculations, shows the molecular packing of the "thin film" polymorph transforms from a slipped one-dimensional (1D) π-stacking motif to a highly oriented and crystalline film upon solvent vapor annealing with a two-dimensional (2D) brick-layer π-stacking arrangment, similar to the so-called "bulk" structure observed in single crystals. We characterize charge transport as a function of vapor annealing, grain orientation, and temperature. Demonstrating that mobility

increases by three orders of magnitude upon solvent vapor annealing and displays a differing temperature-dependent mobility behavior.

1. Introduction

Charge transport in organic semiconductor thin films is greatly affected by small variations in microstructure or molecular packing.[1,2] Even sub-angstrom changes to molecular packing can alter the electronic coupling and thus influence charge carrier mobilities in transistor devices.[3-5] Tuning the molecular packing is normally done through chemical modifications[6], yet these changes can also affect the optoelectronic and physical properties of the material, making fundamental structure-property relations more difficult to quantify and correlate.

Alternatively, adjusting processing conditions provides another approach to altering molecular packing.[7-13] Specific to small molecule systems, processing can be used to access certain thin film polymorphs.[14] Polymorphism, the ability for the same compound to adopt different crystalline packing states, is prevalent in organic semiconductors as the dominant interactions are van der Waals and weak electrostatic interactions.[15] Thus, the fine-tuning of crystal packing and isolation of high mobility polymorphs may be realized through a variety of processing techniques, such as blade or shear coating, thermal annealing, or solvent vapor annealing.[16-18] Furthermore, polymorphism provides an excellent platform in organic semiconductors for examining the fundamental relationship between charge transport and molecular packing as the molecular packing can be varied without the need for chemical modification.[13,17]

In this study, we report a new "thin film" polymorph of N-octyldiisopropylsilyl acetylene bistetracene (BT), accessed via spin coating. Solvent vapor annealing[19-21] transforms this polymorph to the "bulk"

triclinic crystal packing of BT (chemical structure is shown in **Figure 1a**), also observed in single crystals and responsible for the excellent charge carrier mobility in single crystal transistors, due to the 2D "brick-layer" molecular packing.[22] Static and *in-situ* grazing-incidence X-ray diffraction (GIXD) are employed to track the molecular changes within the BT films during exposure to solvent vapors, and through a combination of simulation and crystallographic refinement calculation, we estimate the molecular packing of the thin film polymorph to adopt a slipped 1D π-stacking motif. Organic thin film transistors prepared after solvent vapor annealing result in a remarkable three orders of magnitude increase in carrier mobility. We investigate the transport anisotropy as well as the temperature-dependent mobility. We find the thermally activated transport behavior gives way to one where carrier mobility increases upon decreasing the temperature after phase transformation.

2. Results and Discussion

Figure 1b shows a polarized optical image of a spin-coated film of BT from chloroform on a silicon wafer that exibits little to no birefringence. Upon exposure to chlorobenzene vapors in a closed petri dish, large crystalline domains grow on the order of millimeters from the edge of the substrate and propagate inward, indicating nucleation and growth from the thicker edges[24] (**Figure 1c**). Grazing-incidence X-ray diffraction (GIXD) measurements were performed on the BT film before and after chlorobenzene vapor exposure to help assess the microstructural changes induced by solvent vapor annealing (SVA). The diffraction pattern of the spin-coated BT film is shown in **Figure 1d**, and despite the absence of birefringence in the optical micrographs, the film appears to be highly crystalline and has the characteristics of a 2D powder, where grains are highly oriented out-of-plane, yet randomly oriented in the plane of the film. These diffraction peaks show slight arcing,

indicative of an imperfect 2D powder, with the film having some mosaicity. From the measurement of the diffraction peak position, the unit cell parameters were extracted using a least-square fitting procedure (**Table 1)**.[24,25] The triclinic unit cell of as-cast BT—a=22.80 Å, b=8.03 Å, c=18.24 Å, α=95.6°, β=119.9°, γ= 78.8°—did not match to that of the bulk single crystal, indicating that the film exhibits a new substrate-induced polymorph. These as-cast films even show evidence of additional, competing polymorphs present, with multiple sharp reflections along the q_z axis at $q_{xy} \sim 0$. However, the number of peak positions that could be extracted was not sufficient to index these additional structures.

In order to estimate the molecular packing in the as-cast BT polymorph, crystallographic refinement calculations were performed in which the theoretical X-ray scattering intensities from a test molecular arrangement are fitted to the observed intensities and the best-fit molecular packing is obtained by a Monte Carlo optimization of the fitting error. This procedure has been detailed previously.[24,25] Usually this fitting procedure fixes the molecular structure to a known conformation such as an available bulk molecular structure and only optimizes the positions and Euler angles of the molecules since there are typically not enough intensity data points to fit atomic positions as in single crystal X-ray refinement. However, in the present some conformational flexibility of the BT molecule was introduced by allowing a rotation of the N-octyldiisopropylsilyl acetylene side chains about the triple-bond, similar to what was previously done for TIPS-pentacene.[13] The obtained thin film packing exhibits a slipped one-dimensional (1D) π-stacking motif with a herringbone arrangement of adjacent stacks.

The goodness of the fit is graphically shown in **Figure 2**, where the degree of matching between calculated and measured scattering intensities is shown by pairs of half-circles. While the fit is quite

satisfactory and the obtained packing of the BT cores plausible, the extremely conformationally flexible, large side chains are not well represented by this modeling and the obtained packing should thus be considered the best possible approximation of the molecular packing.

The diffraction pattern after solvent vapor annealing shows a large change in molecular packing, as shown in **Figure 1e**. Using the same least-square-error fitting procedure, the lattice constants were extracted and representative of the bulk single crystal, with the (001) plane normal to the substrate, indicating that BT is packing in an edge-on arrangement. The molecular packing arranges into a 2D brick-like π-stacking motif with close interplanar distances of 3.35 Å. The stacks are characterized by two alternating intermolecular center-to-center distances of 8.59 Å and 8.01 Å between adjacent molecules due to the presence of two translationally inequivalent molecules. The molecular packing of the as-cast and solvent annealed films are shown in **Figure 3**.

To further understand the morphological changes that occur during vapor exposure, *in-situ* solvent vapor annealing GIXD measurements were carried out.[26] A spin-coated film of BT, GIXD image shown in **Figure 4a**, was exposed to chlorobenzene vapors and the diffraction patterns were recorded over time. After 30 minutes, **Figure 4b**, pronounced changes in the diffraction pattern could be observed, as the reflection at q_z = 0.31 $Å^{-1}$ and others representative of the competing polymorph that could not be indexed are no longer present, and only the peaks corresponding to the fitted thin film unit cell appear. The reflections also showed less mosaicity, indicating that the crystalline grains are more ordered. At 60 minutes of exposure, **Figure 4c**, new scattering features began to appear with a distinct Bragg rod forming centered at q_{xy} = 0.72 $Å^{-1}$ corresponding to the bulk BT solvent annealed film. After 300 minutes of solvent annealing, **Figure 4d**, the diffraction

pattern was representative of the bulk triclinic crystal structure and resembled the static solvent annealed BT pattern, with no peaks present corresponding to the as-cast BT diffraction pattern.

Differential scanning calorimetry (DSC) was used to quantify how molecular packing and processing conditions effected the material's thermal properties. We compare BT single crystal, as-cast, and SVA samples as shown in **Figure 5**. Single crystals were grown by slow evaporation from hexane solution.[22] The as-cast and SVA samples are prepared by drop-casting chloroform solution directly into the DSC sample pan (as-cast) followed by exposure to chlorobenzene vapors (SVA) for eight hours. The single crystal (black) shows one sharp endothermic melting transition at 142˚C during the first heating. Cooling from the melt, the single crystal sample exhibits no recrystallization exotherm. Only upon the second heating did we observe a broad 'cold-crystallization'[27-29] exotherm with an onset at 57˚C, followed by a single sharp melting transition at 110˚C. The as-cast sample (blue) demonstrates a single melting endotherm at 106˚C in both the first and second heating ramps and a recrystallization peak at 57˚C during cooling. Finally, the SVA sample shows behavior similar to single crystal with a large melting endotherm at 138˚C during the first heating, recrystallization onset at 57˚C followed by a single melting endotherm at 107˚C.

The first heating curve reveals the crystal phase of these samples. The BT single crystal (black), and SVA (red) samples show similar melting onsets around 140˚C. This supports the conclusions drawn in GIXD analysis which indicates large similarities between the single crystal and SVA microstructures. We attribute the 'cold-crystallization' of the single crystal sample to the slow kinetics of the bulk system. All three samples have a second melting transition (dotted line) around 106-110˚C, indicating that regardless of initial processing conditions, BT adopts the thin film polymorph upon melting and recrystalization under these experimental conditions. GIXD attempts to

observe this transition were inconclusive due to dewetting of films upon melting. In summary, these experimental observations corroborate the GIXD results, as the SVA sample's DSC scans resemble that of the bulk single crystal. Post-processing and polymorph control are also demonstrated as a possible handle to tune a material's thermal properties.

To quantify the effect of molecular packing changes on charge transport within the films, PFBT-treated Au[30], bottom-gate, bottom-contact field-effect transistors were fabricated on 300 nm thermally grown silicon dioxide heavily doped Si wafers. The BT films spin-coated from chloroform solution had hole mobilities of 1.31 x 10^{-4} $cm^2/V{\cdot}s$, threshold voltage of 2.9 V, and an current on/off ratios of 10^2. Transfer and output characteristics are shown in **Figure 6**. Devices measured after solvent vapor annealing showed a significant improvement in performance, with mobilities as high as 0.12 $cm^2/V{\cdot}s$, V_T of -12.6 V, and current on/off ratios of 10^5 for grains parallel to channel, a three orders of magnitude increase in mobility over as-cast devices.

Using the method of crystallization by which crystallization is initated from the edge of the substrate, we fabricated devices with a large range of grain orientations relative to the channel. As carrier mobility in many high performance organic semiconductors is orientation-dependent[31-37], it is critical to study and understand the effect of grain orientation on device performance.[38,39] The solvent annealed film allowed us to conduct a detailed study into the anisotropy of charge transport in bistetracene films. The grain orientation of the films was measured using polarized optical microscopy. In total, over 200 devices were measured, and by plotting the mobility versus the grain orientation, a clear angular dependence of the mobility within bistetracene solvent annealed films is shown in **Figure 7**. The mobility of the films in which the grains were oriented perpendicular to the channel were on average 12 times lower than that of the parallel grain orientation, much larger than

the anisotropy value of 3.4 from the transfer integral calculations[22], similar to mobility anisotropy measurements of single crystals[40], demonstrating the role of grain boundaries at this channel length (50 μm).[41] Yet, this mobility anisotropy compares well to the benchmark two-dimensional brick-layer packing small molecule, TIPS pentacene, which in the solution processed crystalline thin film exhibits mobility anisotropy on the order of 7.5 - 10.[38,42]

To probe how molecular packing and orientation effect the mechanism of charge transport[43], carrier mobility measurements were carried out as a function of temperature. Three different conditions were tested, the first sample was spin-coated and solvent vapor annealed for 30 minutes to isolate the thin film polymorph of BT. The other films were solvent annealed for 8 hours to induce a phase transition to the bulk crystal phase, and devices were tested with grains oriented parallel or perpendicular to the channel. The transistors were measured under vacuum with decreasing temperature ranging from 300 to 100 K in 25 K intervals. The typical temperature dependent mobility for each sample is shown in **Figure 8**. The thin film phase of bistetracene exhibited thermally activated charge transport, with the mobility decreasing in two stages, a steep decline in the high-temperature region (300-200 K), followed by a less drastic decrease in mobility in the low temperature region (100-200 K), with an activation energy of 39 meV obtained from a fitted Arrhenius equation. Contrary to the thin film polymorph of bistetracene, the solvent annealed devices showed an increase in mobility with decreasing temperature in the high temperature range for both the parallel and perpendicular devices. Similar temperature behavior is seen in other high-mobility solution-processed small molecules[44], explained by the intrinsic transport behavior dominated by lattice scattering.[45,46] The parallel devices mobility increased in the temperature range 250 K < T < 300 K, before plateauing between 200K < T < 250 K, and before decreasing upon

further cooling. From the thermally activated low-temperature region, an activation energy of 4.7 meV was calculated. The perpendicular devices showed similar temperature dependent behavior to the parallel devices, with the mobility increasing in the 200 K < T < 300 K, before becoming thermally assisted below 200 K with a slightly higher activation energy of 5.7 meV. Most notably, we measured a non-monotonous temperature dependence[47-50], with a negative temperature coefficient of the mobility for both parallel and perpendicular devices at high temperatures, contrary to the thin film polymorph, which exhibits a thermally activated decrease in mobility with decreasing temperature over the entire investigated range.

3. Conclusion

We observed and characterized a new thin film polymorph of BT which can be converted to a structure similar to the bulk structure of BT using solvent vapor annealing. This transition was monitored using static and *in-situ* GIXD measurements. Field-effect transistors fabricated from the solvent annealed films exhibited three orders of magnitude increase in hole mobility compared to the spin coated films. Using the highly-ordered solvent annealed thin film, we measured the charge transport anisotropy and found it to be similar to the benchmark two-dimensional π-π stacking small molecule, TIPS-pentacene. Temperature dependent mobility measurements also showed a transition from a hopping charge transport mechanism for the thin film polymorph to a lattice scattering behavior in the solvent annealed film. Our experiments highlight the importance of polymorph control and thermal characterization in not just optimizing device performance, but also be as a powerful tool in better understanding the relationship between molecular packing and charge transport mechanism.

4. Experimental Section

Materials: N-octyldiisoproplsilyl acetylene bistetracene (BT) was synthesized according to literature.[22] All solvents were purchased from Sigma Aldrich and used as received.

Thin Film Preparation: Thin films for structural analysis as well as electronic characterization were fabricated by dissolving BT in chloroform (10 mg/ml) followed by spin coating at 2000 rpm for 60 seconds. Solvent annealed samples were placed in a petri dish with a well of 500 µl of chlorobenzene and allowed to crystallize for 8 hours.

Thermal Analysis: Differential scanning calorimetry (DSC) measurements were conducted under N_2 atmosphere at a scan rate of 10^{o}C/min. Standard aluminum crucibles were used. Thin film sample was prepared by drop-casting chloroform BT solution directly into crucible. Solvent-annealed sample was prepared by exposing sample after drop-casting solution to chlorobenzene vapors for eight hours. The sample weight was 4 mg.

Structural Characterization: *In-situ* grazing incidence wide-angle x-ray scattering (GIWAXS) measurements were carried out at D-line (Cornell High Energy Synchrotron Source). A 0.5 × 0.1 mm beam with a wavelength of 1.23 Å and wide band pass (1.47%) was generated from double-bounce multilayer monochromator. The incidence angle was 0.15° with respect to the substrate plane. During X-ray scattering experiments samples were kept in a chamber with vapor pressure control and Kapton windows to allow X-ray scattering through the chamber: liquid solvent was injected into a reservoir at the bottom of the cell. Scattering x-ray photons were detected with a Pilatus 200k pixel array detector (Dectris). Additional GIWAXS experiment were carried out at Stanford

Synchrotron Radiation Lightsource (SSRL) on beamline 11-3 (two-dimensional scattering with an area detector, MAR345 image plate, at grazing incidence). The incident energy was 12.7 keV.

Device Fabrication and Characterization: Bottom-contact, bottom gate devices were fabricated using Si wafers with thermally grown SiO_2 (300 nm thick) were used as the gate and dielectric, respectively, prepatterned with 50 nm Au bottom contacts with a 5 nm Ti adhesion layer. Device channel dimensions of 300 µm and 50 µm for the width and length, respectively, were used. The substrates were sonicated in deionized water and soap, acetone, isopropanol, and deionized water and dried with nitrogen. Substrates were then exposed to UV-ozone treatment for 15 minutes. Electrical device characterization at room temperature was carried out under ambient conditions. Mobility was evaluated in the saturation regime, at a drain voltage V_d = -60 V. Low temperature measurements were carried out under vacuum, at temperatures ranging from 100 to 300 K.

Supporting Information

Supporting Information is available from the Wiley Online Library or from the author.

Acknowledgements

E.K.B., J.L., and A.L.B. acknowledge the National Science Foundation (DMR-1508627) for support of this work. This work is based upon research conducted at the Cornell High Energy Synchrotron Source (CHESS) which is supported by the National Science Foundation under award DMR-1332208.

Received: ((will be filled in by the editorial staff))
Revised: ((will be filled in by the editorial staff))
Published online: ((will be filled in by the editorial staff))

References

[1] V. Coropceanu, J. Cornil, D. A. da Silva Filho, Y. Olivier, R. Silbey, J.-L. Brédas, *Chem. Rev.* **2007**, *107*, 926.

[2] M. Mas-Torrent, C. Rovira, *Chem. Rev.* **2011**, *111*, 4833.

[3] J.-L. Brédas, D. Beljonne, V. Coropceanu, J. Cornil, *Chem. Rev.* **2004**, *104*, 4971.

[4] J.-L. Brédas, J. P. Calbert, D. da Silva Filho, J. Cornil, *Proc. Natl. Acad. Sci. USA* **2002**, *99*, 5804.

[5] J. Cornil, J. P. Calbert, D. Beljonne, R. Silbey, J. Bredas, *Synth. Met.* **2001**, *119*, 1.

[6] C. D. Sheraw, T. N. Jackson, D. L. Eaton, J. E. Anthony, *Adv. Mater.* **2003**, *15*, 2009.

[7] Y. Diao, B. C. K. Tee, G. Giri, J. Xu, D. H. Kim, H. A. Becerril, R. M. Stoltenberg, T. H. Lee, G. Xue, S. C. B. Mannsfeld, Z. Bao, *Nat. Mater.* **2013**, *12*, 665.

[8] G. Giri, R. Li, D.-M. Smilgies, E. Q. Li, Y. Diao, K. M. Lenn, M. Chiu, D. W. Lin, R. Allen, J. Reinspach, S. C. B. Mannsfeld, S. T. Thoroddsen, P. Clancy, Z. Bao, A. Amassian, *Nat. Commun.* **2014**, *5*, 3573.

[9] G. Giri, E. Verploegen, S. C. Mannsfeld, S. Atahan-Evrenk, D. H. Kim, S. Y. Lee, H. A. Becerril, A. Aspuru-Guzik, M. F. Toney, Z. Bao, *Nature* **2011**, *480*, 504.

[10] T. He, M. Stolte, C. Burschka, N. H. Hansen, T. Musiol, D. Kälblein, J. Pflaum, X. Tao, J. Brill, F. Würthner, *Nat. Commun.* **2015**, *6*, 5954.

[11] T. Matsukawa, M. Yoshimura, M. Uchiyama, M. Yamagishi, A. Nakao, Y. Takahashi, J. Takeya, Y. Kitaoka, Y. Mori, T. Sasaki, *Jpn. J. Appl. Phys.* **2010**, *49*, 085502.

[12] C. C. Mattheus, A. B. Dros, J. Baas, G. T. Oostergetel, A. Meetsma, J. L. de Boer, T. T. Palstra, *Synth. Met.* **2003**, *138*, 475.

[13] Y. Diao, K. M. Lenn, W.-Y. Lee, M. A. Blood-Forsythe, J. Xu, Y. Mao, Y. Kim, J. A. Reinspach, S. Park, A. Aspuru-Guzik, G. Xue, P. Clancy, Z. Bao, S. C. B. Mannsfeld, *J. Am. Chem. Soc.* **2014**, *136*, 17046.

[14] A. O. Jones, B. Chattopadhyay, Y. H. Geerts, R. Resel, *Adv. Funct. Mater.* **2016**.

[15] H. Chung, Y. Diao, *J. Mater. Chem. C* **2016**, *4*, 3915.

[16] A. M. Hiszpanski, R. M. Baur, B. Kim, N. J. Tremblay, C. Nuckolls, A. R. Woll, Y.-L. Loo, *J. Am. Chem. Soc.* **2014**, *136*, 15749.

[17] O. D. Jurchescu, D. A. Mourey, S. Subramanian, S. R. Parkin, B. M. Vogel, J. E. Anthony, T. N. Jackson, D. J. Gundlach, *Phys. Rev. B* **2009**, *80*, 085201.

[18] G. E. Purdum, N. Yao, A. Woll, T. Gessner, R. T. Weitz, Y. L. Loo, *Adv. Funct. Mater.* **2016**, *26*, 2357.[19] K. C. Dickey, J. E. Anthony, Y. L. Loo, *Adv. Mater.* **2006**, *18*, 1721.

[20] H. Ullah Khan, R. Li, Y. Ren, L. Chen, M. M. Payne, U. S. Bhansali, D.-M. Smilgies, J. E. Anthony, A. Amassian, *ACS Appl. Mater. Interfaces* **2013**, *5*, 2325.

[21] W. H. Lee, D. H. Kim, J. H. Cho, Y. Jang, J. A. Lim, D. Kwak, K. Cho, *Appl. Phys. Lett.* **2007**, *91*, 092105.

[22] L. Zhang, A. Fonari, Y. Liu, A.-L. M. Hoyt, H. Lee, D. Granger, S. Parkin, T. P. Russell, J. E. Anthony, J.-L. Brédas, V. Coropceanu, A. L. Briseno, *J. Am. Chem. Soc.* **2014**, *136*, 9248.

[23] L. Yu, M. R. Niazi, G. O. N. Ndjawa, R. Li, A. R. Kirmani, R. Munir, A. H. Balawi, F. Laquai, A. Amassian, *Sci. Adv*. **2017**, *3*, 1.

[24] S. C. Mannsfeld, M. L. Tang, Z. Bao, *Adv. Mater.* **2011**, *23*, 127.

[25] S. C. Mannsfeld, A. Virkar, C. Reese, M. F. Toney, Z. Bao, *Adv. Mater.* **2009**, *21*, 2294.

[26] A. Amassian, V. A. Pozdin, R. Li, D.-M. Smilgies, G. G. Malliaras, *J. Mater. Chem.* **2010**, *20*, 2623.

[27] M. O. Ahmed, C. Wang, P. Keg, W. Pisula, Y.-M. Lam, B. S. Ong, S.-C. Ng, Z.-K. Chen, S. G. Mhaisalkar, *J. Mater. Chem.* **2009**, *19*, 3449.

[28] W. H. Lee, J. A. Lim, D. H. Kim, J. H. Cho, Y. Jang, Y. H. Kim, J. I. Han, K. Cho, *Adv. Funct. Mater.* **2008**, *18*, 560.

[29] J. Y. Kim, T. Yasuda, Y. S. Yang, N. Matsumoto, C. Adachi, *Chem. Commun.* **2014**, *50*, 1523.

[30] H. Lee, Y. Zhang, L. Zhang, T. Mirabito, E. K. Burnett, S. Trahan, A. R. Mohebbi, S. C. Mannsfeld, F. Wudl, A. L. Briseno, *J. Mater. Chem. C* **2014**, *2*, 3361.

[31] V. Podzorov, E. Menard, A. Borissov, V. Kiryukhin, J. Rogers, M. Gershenson, *Phys. Rev. Lett.* **2004**, *93*, 086602.

[32] V. C. Sundar, J. Zaumseil, V. Podzorov, E. Menard, R. L. Willett, T. Someya, M. E. Gershenson, J. A. Rogers, *Science* **2004**, *303*, 1644.

[33] J. Rivnay, L. H. Jimison, J. E. Northrup, M. F. Toney, R. Noriega, S. Lu, T. J. Marks, A. Facchetti, A. Salleo, *Nat. Mater.* **2009**, *8*, 952.

[34] C. W. Sele, B. Kjellander, B. Niesen, M. J. Thornton, J. Van der Putten, K. Myny, H. J. Wondergem, A. Moser, R. Resel, A. J. van Breemen, N. van Aerle, P. Heremans, J. E. Anthony, G. H. Gelinck, *Adv. Mater.* **2009**, *21*, 4926.

[35] R. Li, L. Jiang, Q. Meng, J. Gao, H. Li, Q. Tang, M. He, W. Hu, Y. Liu, D. Zhu, *Adv. Mater.* **2009**, *21*, 4492.

[36] M. J. Lee, D. Gupta, N. Zhao, M. Heeney, I. McCulloch, H. Sirringhaus, *Adv. Funct. Mater.* **2011**, *21*, 932.

[37] C. Reese, Z. Bao, *Adv. Mater.* **2007**, *19*, 4535.

[38] R. L. Headrick, S. Wo, F. Sansoz, J. E. Anthony, *Appl. Phys. Lett.* **2008**, *92*, 063302.

[39] L. H. Jimison, M. F. Toney, I. McCulloch, M. Heeney, A. Salleo, *Adv. Mater.* **2009**, *21*, 1568.

[40] C. Reese, Z. Bao, *Adv. Mater.* **2007**, *19*, 4535.

[41] L. Yu, X. Li, J. Smith, S. Tierney, R. Sweeney, B. C. Kjellander, G. H. Gelinck, T. D. Anthopoulos, N. Stingelin, *J. Mater. Chem.* **2012**, *22*, 9458.

[42] J. Wade, F. Steiner, D. Niedzialek, D. T. James, Y. Jung, D.-J. Yun, D. D. Bradley, J. Nelson, J.-S. Kim, *J. Mater. Chem. C* **2014**, *2*, 10110.

[43] Q.-J. Sun, X. Gao, S.-D. Wang, *J. Appl. Phys.* **2013**, *113*, 194506.

[44] A. Y. Meneau, Y. Olivier, T. Backlund, M. James, D. W. Breiby, J. W. Andreasen, H. Sirringhaus, *Adv. Funct. Mater.* **2016**, *26*, 2326.

[45] D. Chirvase, Z. Chiguvare, M. Knipper, J. Parisi, V. Dyakonov, J. Hummelen, *J. Appl. Phys.* **2003**, *93*, 3376.

[46] S. Terao, T. Hirai, N. Morita, H. Maeda, K. Kojima, M. Tachibana, *J. Appl. Phys.* **2010**, *108*, 124511.

[47] N. A. Minder, S. Ono, Z. Chen, A. Facchetti, A. F. Morpurgo, *Adv. Mater.* **2012**, *24*, 503.

[48] R. Pfattner, M. Mas-Torrent, I. Bilotti, A. Brillante, S. Milita, F. Liscio, F. Biscarini, T. Marszalek, J. Ulanski, A. Nosal, M. Gazicki-Lipman, M. Leufgen, G. Schmidt, L. W. Molenkamp, V. Laukhin, J. Veciana, C. Rovira, *Adv. Mater.* **2010**, *22*, 4198.

[49] T. Sakanoue, H. Sirringhaus, *Nat. Mater.* **2010**, *9*, 736.

[50] X. Xu, Y. Yao, B. Shan, X. Gu, D. Liu, J. Liu, J. Xu, N. Zhao, W. Hu, Q. Miao, *Adv. Mater.* **2016**, *28*, 5276.

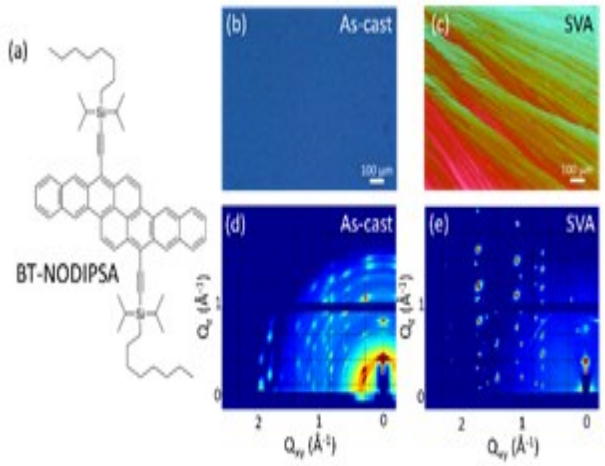

Figure 1. a) Chemical structure of BT, (b) optical image of a spin-coated film of BT, and (c) polarized optical image of BT film after solvent vapor annealing. (d) 2D-GIXD patterns of the as-cast BT and (e) SVA films.

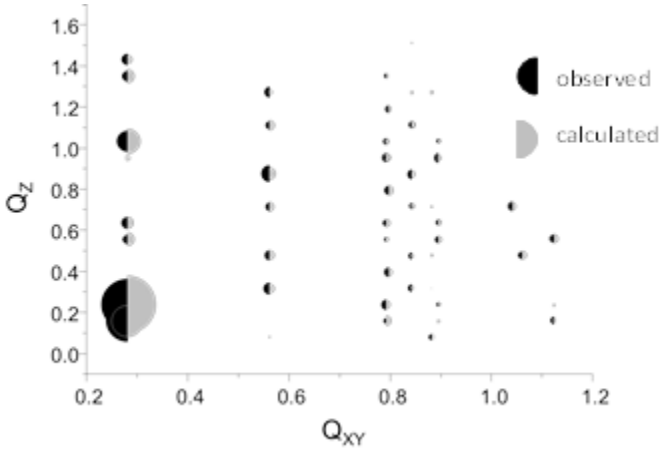

Figure 2. The measured and calculated diffraction intensities (best-fit) for the spin coated BT film.

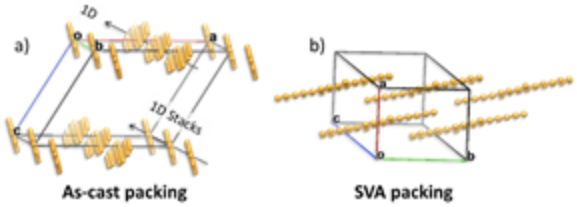

Figure 3. Crystal structure and molecular packing of (a) as-cast BT polymorph. The 1D pi-stacks crystallize along the b-axis (010). (b) The solvent vapor annealed BT molecular packing is identical to the bulk crystal structure (2D brick layer motif). Note: the silylethynyl solubilizing groups have been removed for clarity.

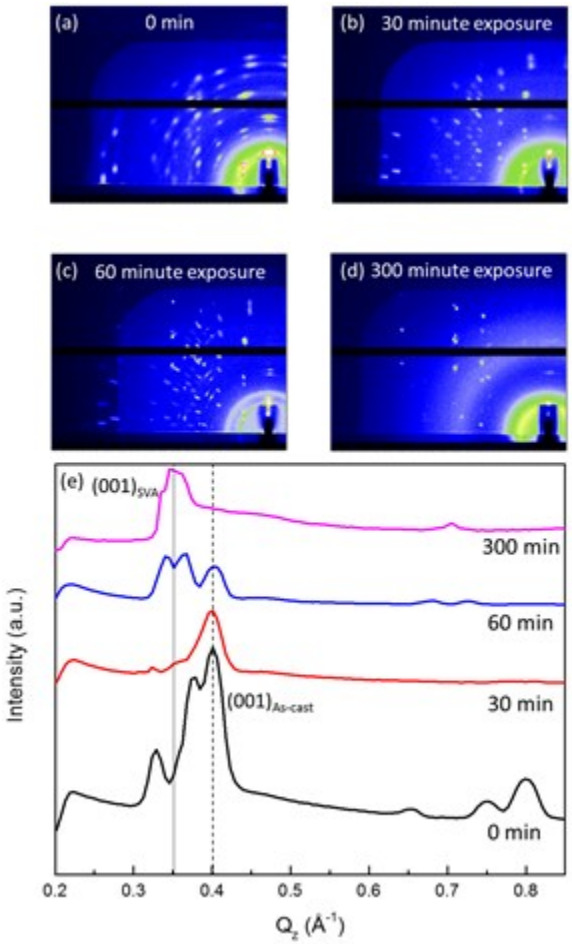

Figure 4. In-situ GIXD patterns of (a) spin-coated BT film before exposure to chlorobenzene vapors. (b) Film after 30 minutes, (c) 60 minutes, and (d) 300 minutes of SVA. (e) Out-of-plane intensity plots with lines to guide the eye along the major diffraction peak of the as cast (dashed) and static solvent annealed films

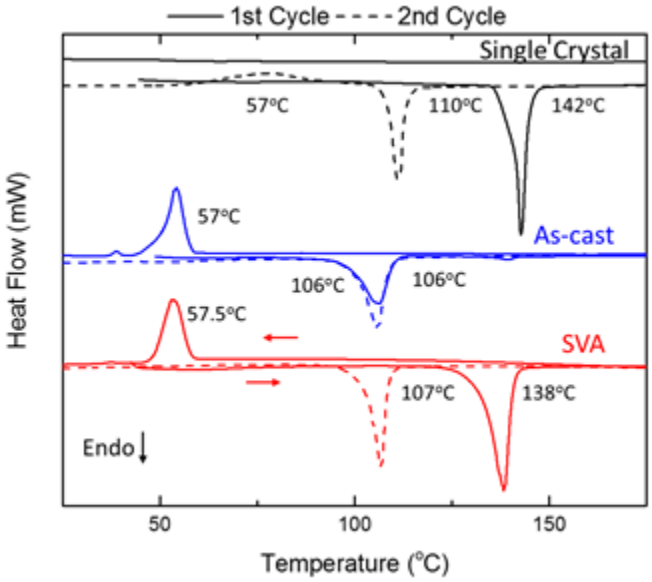

Figure 5. Heating (solid), cooling (solid), and 2nd heating (dashed) thermograms of BT in the single crystal (black), drop casted (blue), and solvent vapor annealed (red); heating rate, 10 ˚C/min.

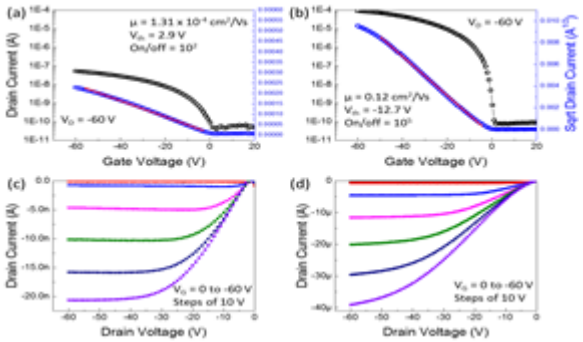

Figure 6. (a) Transfer characteristics in the saturated region of the as cast BT film and (b) SVA film. (c) Output characteristics of the as cast BT and (d) SVA film.

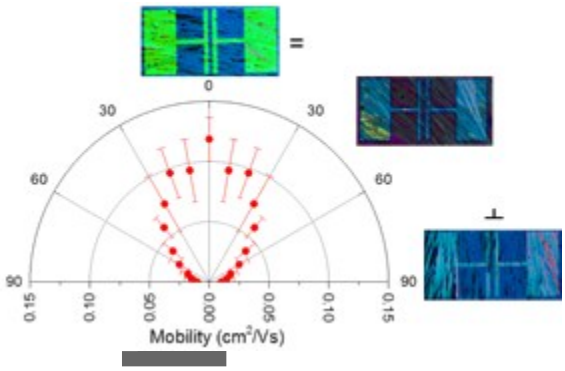

Figure 7. Polar plot of the hole mobility versus grain orientation angle of solvent vapor annealed BT film. The mobility data is reported from 0˚ to 90˚ and reflected to show the expected behavior over 180˚. Devices with grains oriented at 0˚ are denoted as parallel, and grains oriented 90˚ to the channel are denoted as perpendicular

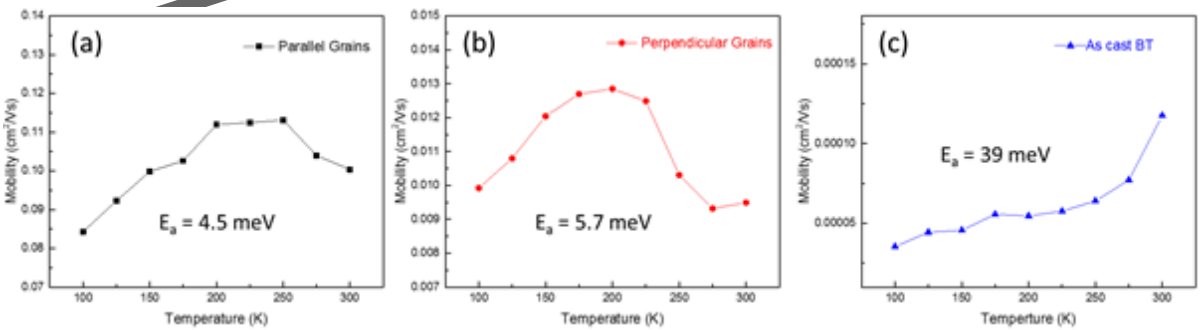

Figure 8. Temperature-dependent saturation mobility (V_D = -60 V) measured in 50 µm channel of (a) solvent-annealed parallel grains, (b) perpendicular grains, and (c) as cast film. The activation energies (E_a) extracted in the trap dominated regimes are also given.

Table 1. Lattice constants of as-cast and solvent annealed unit cells with bulk crystal structure included for reference.

Processing Condition	a (Å)	b (Å)	c (Å)	α (˚)	β (˚)	γ (˚)
As-cast	22.80	8.03	18.20	95.6˚	119.9˚	78.8˚
Solvent annealed	11.76	12.89	18.75	97.6˚	106.4˚	95.7˚
Bulk single crystal	11.76	12.89	18.75	97.6˚	106.4˚	95.7˚

A bistetracene thin-film polymorph is accessed by spin-coating and the molecular packing is characterized utilizing crystallographic refinement calculations. Solvent-vapor annealing converts the film from 1D π-stacking motif to the bulk-crystal 2D "brick-layer" packing. Temperature-dependent mobility demonstrates a transition from a hopping charge transport mechanism in the thin film polymorph to a lattice-scattering dominated behavior in the solvent annealed film.

organic semiconductors, polymorphism, bistetracene, solvent vapor annealing

Edmund K. Burnett, Jack Ly, Muhammad R. Niazi, Lei Zhang, Samantha McCluskey, Aram Amassian, Detlef-M. Smilgies, Stefan C. B. Mannsfeld, and Alejandro L. Briseno*

Bistetracene Thin Film Polymorphic Control to Unravel the Effect of Molecular Packing on Charge Transport